

Reconstruction of physics objects in the CMS detector

Aruna Kumar Nayak^{*†}

IRFU, CEA, Saclay, France E-mail: Aruna.Nayak@cern.ch

The reconstruction and identification of physics objects in the CMS detector, in the context of the charged Higgs boson search analysis, are presented. The reconstruction algorithms and their performance in 7 TeV and 8 TeV LHC data are discussed. The identification of tau hadronic decays, the reconstruction of hadronic jets and missing transverse energy and the identification of b jets are described in detail.

*Prospects for Charged Higgs Discovery at Colliders - Charged 2012,
October 8-11, 2012
Uppsala University, Sweden*

^{*}Speaker.

[†]On behalf of CMS Collaboration

1. Introduction

Some extensions of the Standard Model of Particle Physics, such as the Minimal Supersymmetric Standard Model (MSSM) or the Two Higgs Doublet Model, predict the presence of charged Higgs bosons. For large values of $\tan\beta$, the ratio of the vacuum expectation values of the two Higgs doublets, the charged Higgs decays to a tau lepton and a neutrino. The CMS experiment at CERN [1] has performed the search for a light charged Higgs boson decaying to $\tau\nu_\tau$ using 7 TeV LHC data [2]. The search requires efficient identification of τ -leptons as well as a good reconstruction of hadronic jets, missing transverse energy and a good b jet identification.

The CMS experiment has developed excellent techniques for the reconstruction and identification of physics objects. In this article, the CMS reconstruction and identification techniques are briefly discussed in order of their importance to the charged Higgs search analysis. Many physics analyses at CMS use high level physics objects reconstructed using the particle-flow event reconstruction technique. A brief description of the particle-flow event reconstruction is presented below.

2. Particle-Flow Event Reconstruction

The particle-flow event reconstruction algorithm aims at reconstructing all stable particles in the event by combining information from all CMS sub-detectors. The algorithm optimizes the determination of particle types, directions and their energies. The resulting list of particles are then used to reconstruct higher level objects such as jets, taus, missing transverse energy, to compute charged lepton and photon isolation, etc. The details of the particle-flow event reconstruction developed at CMS can be found in [3].

The basic elements of the particle-flow event reconstruction are the charged particle tracks reconstructed in the central tracker and the energy clusters reconstructed in electromagnetic and hadronic calorimeters. The charged particle tracks are reconstructed using an iterative tracking strategy, described in [4], with both a high efficiency and a low fake rate for charged particle momentum as low as 150 MeV/c. The energy clustering is performed in each sub-detector of the calorimeters separately using a specific clustering algorithm, developed for particle-flow event reconstruction, which aims for a high detection efficiency even for low energy particles and separation of close energy deposits. These basic elements are then connected to each other using a link algorithm to fully reconstruct each single particle, while removing any possible double counting from different detectors. The algorithm produces “blocks” of elements linked directly or indirectly. The particle-flow algorithm described in [4] is finally used to reconstruct and identify a set of particles from each block of elements. Charged hadrons are reconstructed from the tracks in the central tracker. Photons and neutral hadrons are reconstructed from energy clusters in calorimeters. Clusters separated from the extrapolated position of tracks in the calorimeters constitute a clear signature of these neutral particles. A neutral particle overlapping with charged particles in the calorimeters can be detected as a calorimeter energy excess with respect to the sum of the associated track momenta. The resulting list of reconstructed particles constitute a global description of each event, available for subsequent physics analysis.

3. Hadronic Jets

Quarks and gluons produced in hard scattering of partons in pp collisions manifest themselves as hadronic jets. A detailed understanding of the jet energy calibration and resolution is of crucial importance and is a leading source of uncertainty for many analyses with jets in the final state. A brief description of CMS jet reconstruction algorithms, jet energy calibration techniques and the jet energy scale uncertainties are presented here.

3.1 Reconstruction of Hadronic Jets

Four types of jets are reconstructed at CMS depending on the input to the jet clustering algorithm: calorimeter jets, Jet-Plus-Track (JPT) jets, Particle-Flow (PF) jets, and track jets [5]. Jets presented here are reconstructed using the anti- k_T [6] clustering algorithm with the size parameter $R = 0.5$. To evaluate their performance, in Monte Carlo simulations, generated jets (GenJets) or particle jets are reconstructed as well by applying the same jet clustering algorithm to all stable generated particles. Since most of the analysis at CMS are using PF jets, we concentrate here on PF jets while briefly describing two other types of jets.

Calorimeter jets are reconstructed using energy deposits in the calorimeter towers, where calorimeter tower consists of one or more hadronic calorimeter (HCAL) cells and the geometrically corresponding electromagnetic (ECAL) crystals. The *Jet-Plus-Track* algorithm [7] exploits the excellent performance of the CMS tracking detectors to improve the p_T response and resolution of calorimeter jets. For each track in the jet, the average expected calorimeter energy is subtracted and the momentum measured in the tracker is added to the jet. For the tracks which are bent out of the jet cone due to magnetic field the momentum of the track is added to the jet. PF jets are reconstructed from the list of particles reconstructed using particle-flow algorithm. The jet momentum and spacial resolutions are improved with respect to the calorimeter jets, since the use of tracking detectors and excellent ECAL granularity allows to resolve and precisely measure charged hadrons and photons inside jets.

3.2 Energy Calibration of Hadronic Jets

Due to the non-uniform and non-linear response of the CMS calorimeters the jet energy measured in the detector is typically different from the corresponding particle jet energy. Furthermore, electronic noise and additional pp interactions in the same bunch crossing (event pile-up) leads to extra unwanted energy. The purpose of the jet energy correction is to relate, on average, the energy measured for the detector jet to the energy of the corresponding particle jet.

CMS has developed a factorized multi-step procedure for the jet energy calibration (JEC) [8]. The correction is applied as a multiplicative factor to each component of the raw jet four momentum vector p_μ^{raw} as shown in Eq.3.1.

$$p_\mu^{corrected} = p_\mu^{raw} \cdot C_{offset}(p_T^{raw}) \cdot C_{MC}(p_T', \eta) \cdot C_{rel}(\eta) \cdot C_{abs}(p_T'') \quad (3.1)$$

where p_T' is the transverse momentum of the jet after applying offset correction and p_T'' is the transverse momentum of the jet after all previous corrections. C_{offset} is the offset correction derived using the jet area method [8]. For each event, an average p_T density ρ per unit area is estimated,

which characterizes the soft jet activity and is contamination of the underlying event, the electronic noise and the pile-up. The MC calibration, C_{MC} , is based on the simulation and corrects the energy of the reconstructed jets such that it is equal to the energy of generated MC particle jets. It removes the bulk of the non-uniformity in η and the non-linearity in p_T . The residual corrections C_{rel} and C_{abs} for the relative and absolute energy scales, respectively, are derived using data driven method, using dijet and γ/Z +jets events, to account for the small differences between data and simulation. Fig. 1 (left) shows the data/MC ratio for the absolute jet energy scale as function of p_T of the reference object. The uncertainty due to various sources are shown in Fig. 1 (right) as function of jet p_T . The uncertainty due to pile-up dominates at low p_T .

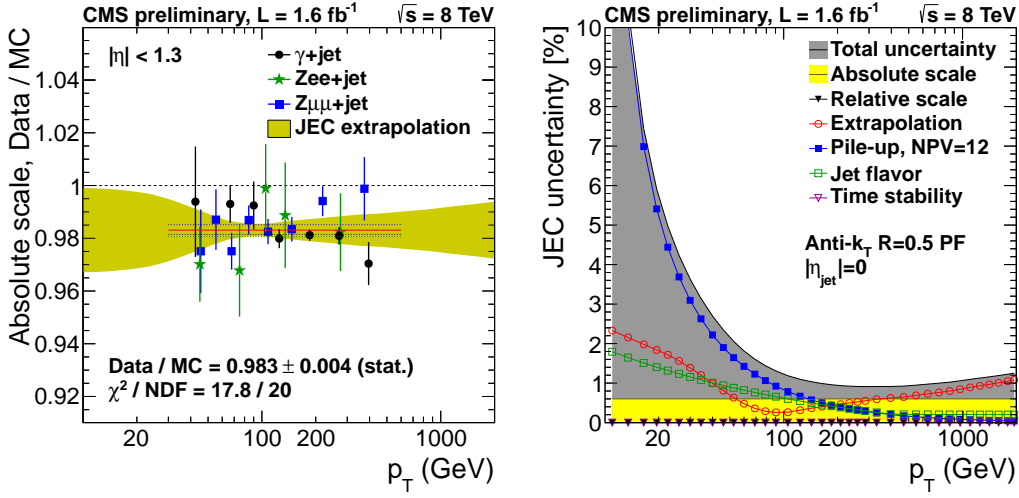


Figure 1: Left: Data/MC ratio of absolute jet energy scale as function p_T of reference object. Right: Difference sources of JEC uncertainties as function of jet p_T .

4. Reconstruction of Hadronic Tau Decays

The τ lepton is the heaviest among the three Standard Model leptons and has a very short lifetime. Thus it decays before reaching the detector elements. In two thirds of the cases, τ leptons decay hadronically, typically into one or three charged mesons (predominantly π^+ , π^-), often accompanied by neutral pions and a ν_τ . The algorithm designed at CMS uses particle-flow particles, such as final state photons and charged hadrons, to identify hadronic decays of τ leptons (τ_h) through the reconstruction of the intermediate resonances. The ν_τ escapes undetected and is not considered in the τ_h reconstruction.

4.1 τ_h Identification Algorithm

The algorithm used at CMS to reconstruct and identify hadronic τ decays is called Hadron Plus Strip (HPS) algorithm [9]. The algorithm uses PF jets, reconstructed using anti- k_T algorithm with a distance parameter $R=0.5$, as an initial seed. The algorithm first reconstructs the π^0 components of the τ_h , then combines them with the charged hadrons to reconstruct the tau decay mode and calculate tau four-momentum and isolation quantities. Special attention is given to photon conversions in the CMS tracker material. The photons are reconstructed in "strips", objects that are built

out of electromagnetic particles (PF photons and electrons), to take into account the broadening of calorimeter energy deposit due to the bending of electron/positron tracks in the CMS magnetic field. Strips satisfying a minimum transverse momentum requirement of $p_T^{strip} > 1 \text{ GeV}/c$ are finally combined with the charged hadrons to reconstruct individual decay modes. The following decay topologies are considered by the algorithm:

1. *Single Hadron* corresponds to $h^- \nu_\tau$ and $h^- \pi^0 \nu_\tau$ decays in which the neutral pions have too little energy to be reconstructed as strips.
2. *One hadron + one strip* reconstructs the decay mode $h^- \pi^0 \nu_\tau$ in events where the photons from π^0 decay are close together on the calorimeter surface.
3. *One hadron + two strips* corresponds to the decay mode $h^- \pi^0 \nu_\tau$ in events where photons from π^0 decay are well separated.
4. *Three hadrons* corresponds to the decay mode $h^- h^+ h^- \nu_\tau$. The three prong charged hadrons are required to come from the same secondary vertex.

No separate decay topologies are considered for the $h^- \pi^0 \pi^0$ and $h^- h^+ h^- \pi^0 \nu_\tau$ decay modes and they are reconstructed via the existing topologies. All charged hadrons and strips are required to be contained within a cone of size $\Delta R = (2.8 \text{ GeV}/c)/p_T^{\tau_h}$, where $p_T^{\tau_h}$ is the transverse momentum of the reconstructed τ_h . The four-momenta of charged hadrons and strips are reconstructed according to the respective τ_h decay topology hypothesis, assuming all charged hadrons to be pions, and are required to be consistent with the masses of the intermediate meson resonances.

The reconstructed τ_h candidates are required to be isolated. The isolation for τ_h candidates are computed using two approaches: cut based and multivariate analysis techniques. The cut based isolation criteria requires that the sum p_T of charged hadrons and photons present within the isolation cone of size $\Delta R = 0.5$ around the direction of the τ_h , apart from the τ_h decay products, is less than a certain threshold. In order to reduce the dependency of the isolation on the event pile-up, the charged hadrons which are originating from the same primary vertex as that of the leading charged hadron of the τ_h are considered for isolation. A correction ($\delta\beta$ correction) is applied to account for the neutral component of the pile-up in the isolation cone. The neutral component of the pile-up in the isolation cone is estimated as the sum p_T of charged hadrons in the isolation cone originating from the pile-up vertices multiplied by the expected ratio of charged hadrons to the neutral hadrons. The estimated neutral component due to pile-up is subtracted from the isolation $\sum p_T$. By adjusting the threshold on isolation $\sum p_T$, three working points, “loose”, “medium”, and “tight” are defined. The “loose” working point corresponds to a probability of approximately 1% for QCD jets to be misidentified as τ_h . In the MVA approach, the isolation $\sum p_T$ is computed in annular rings around the τ_h candidates using the same PF particles used for cut based isolation. A boosted decision tree (BDT) is trained against the QCD jets. Three working points, “loose”, “medium”, and “tight” are defined depending on the cuts on the BDT output.

4.2 Performance of τ_h Identification

The efficiency of the τ_h reconstruction and identification is measured from data using a tag and probe method with a sample of $Z \rightarrow \tau\tau \rightarrow \mu\tau_h$ events. The events are preselected using kinematic

cuts and a set of requirements to suppress the background from $Z \rightarrow \mu\mu$, W , and QCD events, but without applying the τ_h -identification algorithm. The isolated muon is used as tag while an isolated jet candidate with a leading track above a certain threshold is considered as probe. The muon and the leading track in the jet are required to be of opposite charges. The HPS τ_h -identification algorithm is applied to the jet in the preselected events. The invariant mass distribution of the muon-jet system for those events that pass or fail the τ_h -identification are then fitted using signal and background distributions provided by MC simulation to extract the τ_h identification efficiency. The systematic uncertainties of the measured tau identification efficiency depend on the uncertainty arising from the template fit and the preselection efficiency. The total uncertainty is about 6-7%. Fig. 2 shows the expected τ_h identification efficiency as function of the generated visible τp_T estimated from $Z \rightarrow \tau\tau$ MC events for reconstructed τ_h threshold of 20 GeV/c. The efficiency has little dependence on the tau p_T and the number of primary vertices, which shows the stability of the tau identification algorithm with event pile-up.

The mis-identification probability of quark and gluon jets as τ_h have been measured from data using “W+jets” and di-jet enriched events. The jet $\rightarrow \tau_h$ mis-identification probability estimated from data and MC agree within approximately 20%.

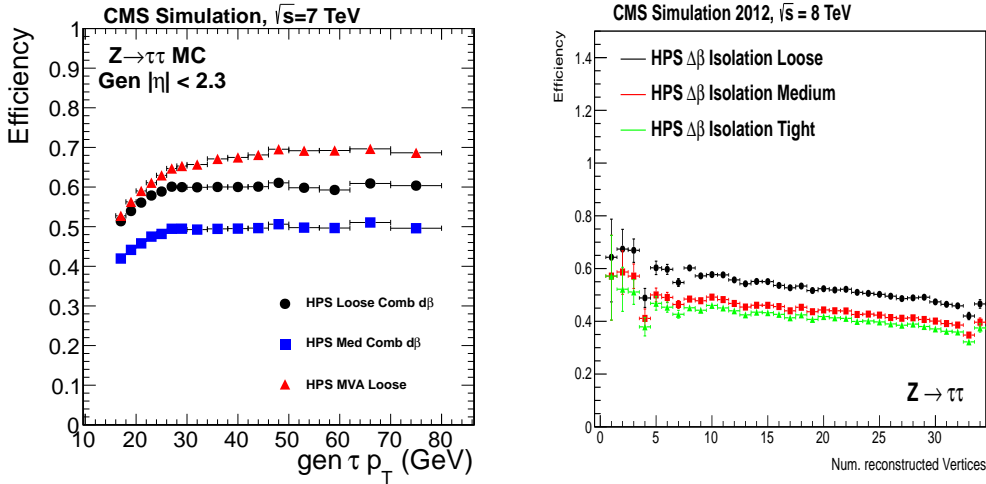


Figure 2: Expected tau identification efficiency for different isolation working points as function of generated tau p_T (left) and number of primary vertices (right).

4.3 Discrimination Against Electrons and Muons

Isolated electrons and muons passing the τ_h identification and isolation criteria are also important source of backgrounds in many analyses with τ_h in the final state. Muons reconstructed as τ_h are rejected using tracking information in the muon detectors and energy deposit in the calorimeter. With simple cut based criteria, the $\mu \rightarrow \tau_h$ mis-identification probability is reduced to less than 1% while keeping $\sim 99\%$ efficiency for real taus. To reduce the $e \rightarrow \tau_h$ mis-identification probability a multivariate discriminant is used. A BDT is trained using input variables such as the τ position and momentum variables, cluster shape variables of PF photons, and tracking and cluster shape variables representing the compatibility of the leading charged hadron to be an electron. The $e \rightarrow \tau_h$

mis-identification probability is reduced to only a few percent while keeping the efficiency for real taus above 80%. The $e \rightarrow \tau_h$ and $\mu \rightarrow \tau_h$ mis-identification probabilities are measured also from data using $Z \rightarrow ee$ and $Z \rightarrow \mu\mu$ enriched events.

5. Reconstruction of Missing Transverse Momentum

The missing transverse momentum, E_T^{miss} , is reconstructed as the negative of the vector sum of the transverse momenta of all final-state particles reconstructed in the detector. There are three distinct algorithms developed in CMS to reconstruct E_T^{miss} : PF E_T^{miss} , Calo E_T^{miss} , and TC E_T^{miss} [10]. PF E_T^{miss} is calculated from the reconstructed PF particles, Calo E_T^{miss} is calculated using the energies contained in calorimeter towers and their direction, relative to the center of the detector, to define pseudo-particles, and TC E_T^{miss} is based on Calo E_T^{miss} , but the response and resolution is improved using tracks reconstructed in the inner tracker.

A three-step correction is devised to remove the bias in the E_T^{miss} scale due to the non-linearity of the response of the calorimeter for neutral and charged hadrons, caused by event pile-up, large bending of low p_T tracks due to strong magnetic field in CMS, etc.. The correction procedure relies on the fact that E_T^{miss} can be factorized into contributions from jets, isolated high p_T photons, electrons, muons and unclustered energies. The jet energy scale corrections are propagated to E_T^{miss} using the so called "type-I" correction:

$$E_{x,y}^{miss,corrected} = E_{x,y}^{miss,raw} - \sum_i \left(P_{i,(x,y)}^{corrected\ jets} - P_{i,(x,y)}^{raw\ jets} \right) \quad (5.1)$$

In order to correct for the soft jets below the threshold used for "type-I" correction and energy deposits not clustered in any jet, a second correction can be applied to the unclustered energy, which is called "type-II" correction. This correction is obtained from $Z \rightarrow ee$ events, as discussed in [10]. To reduce the dependency of E_T^{miss} on event pile-up, a so called "type-0" correction has been developed only for PF E_T^{miss} . For each pile-up vertex the expected missing neutral momentum is calculated using an improved PF candidate to vertex association technique and added it vectorially to PF E_T^{miss} .

5.1 E_T^{miss} Scale and Resolution

The performance of E_T^{miss} is studied using events containing a Z boson where the E_T^{miss} can be induced by removing the vector boson from the event. The well measured Z boson, from two electrons or two muons, provides the momentum scale, q_T and a unique event axis, \hat{q}_T . The hadronic recoil, \vec{u}_T , is defined as the vector sum of the transverse momenta of all particles except the vector boson. Momentum conservation in the transverse plane requires $\vec{q}_T + \vec{u}_T = 0$. The projection of the hadronic recoil onto the axis \hat{q}_T yields two signed components, parallel ($u_{||}$) and perpendicular (u_{\perp}) to the event axis, where $u_{||}$ is typically negative. The mean value of the scalar quantity $\langle u_{||} \rangle / q_T$ is the correction factor required for E_T^{miss} measurements and is closely related to jet energy scale corrections. $\langle u_{||} \rangle / q_T$ is referred as response. Fig. 3 shows the response curve versus q_T for 2012 early run data and MC simulation. Deviations of the response curve from unity probe the E_T^{miss} response as function of q_T . The E_T^{miss} resolution is measured as the RMS spread of $u_{||}$ and

u_{\perp} about their mean values, after correcting for the response. Fig. 3 shows the E_T^{miss} resolution as function of the number of primary vertices.

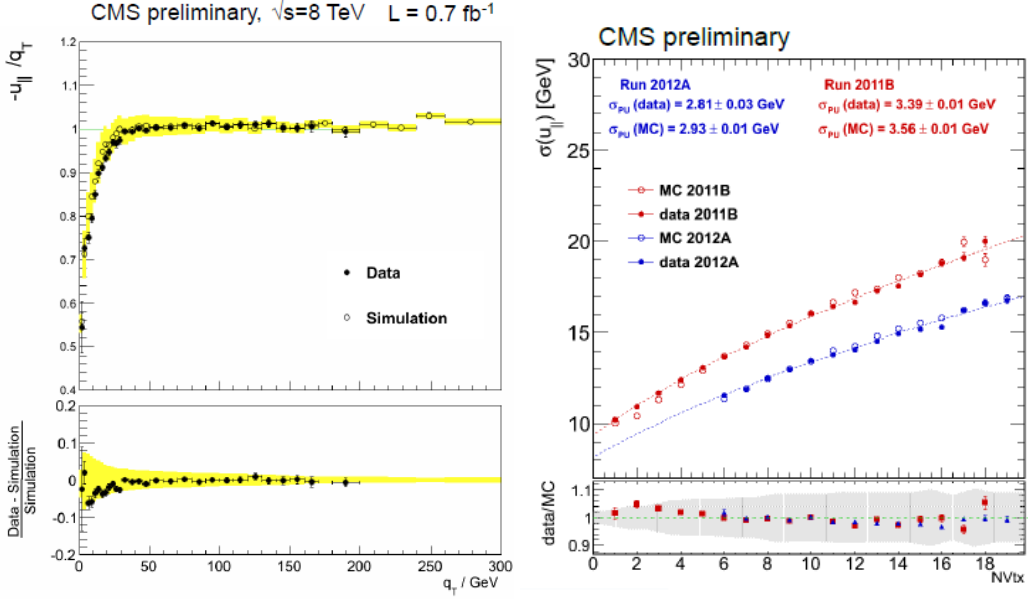


Figure 3: Left: The E_T^{miss} response measured in $Z \rightarrow \mu\mu$ events. Right: The E_T^{miss} resolution as function of the number of primary vertices. The resolution is better in 2012 early run (2012A) data compared to 2011 data (2011B) due to improved energy reconstruction in electromagnetic and hadronic calorimeter to reduce the effects of the out-of-time pile-up interactions.

6. b-Jet Identification

The properties of the b-hadrons are used to identify hadronic jets originating from the fragmentation of b-quarks. These hadrons have relatively large masses, long lifetimes, and daughter particles with hard momentum spectra. Their semileptonic decays can be exploited as well. Various b-tagging algorithms used at CMS and their performance are briefly discussed here.

6.1 b-Tagging Algorithms

CMS has developed a variety of algorithms to identify b-quarks based on variables such as the impact parameter of charged particle tracks, the properties of reconstructed decay vertices, and the presence of a lepton, or the combination of the above information [11]. Each of these algorithms produces a single discriminator value for each jet. The minimum thresholds on these discriminators define loose (“L”), medium (“M”), and tight (“T”) working points corresponding to the mis-identification probability for light parton jets of approximately 10%, 1%, and 0.1%, respectively, at an average jet p_T of 80 GeV/c.

The impact parameter (IP) of a track with respect to the primary vertex is calculated in three dimensions by taking the advantage of the excellent resolution of the pixel detector along the z axis. The sign of the IP is defined as the sign of the scalar product of the vector pointing from the primary vertex to the point of closest approach with the jet direction. While the IP values of the tracks

originating from the decay of particles traveling along the jet axis tend to have positive values, the IP of prompt tracks can have positive or negative values. The impact parameter significance S_{IP} , defined as the ratio of the IP to its estimated uncertainty, is used as a discriminating observable. The simplest algorithm based on the track impact parameter is called *Track Counting* (TC) algorithm which sorts tracks in a jet by decreasing values of IP significance. The *Track Counting High Efficiency* (TCHE) and *Track Counting High Purity* (TCHP) algorithms use the S_{IP} of second and third ranked track as the discriminator value. The IP information of several tracks in a jet are also combined to provide better discriminating power. The *Jet Probability* (JP) algorithm uses an estimate of the likelihood that all tracks associated to the jet come from the primary vertex. The *Jet B Probability* (JBP) algorithm gives more weight to the tracks with the highest IP significance, up to a maximum of four such tracks, which matches the average number of reconstructed charged particles from the b-hadron decays.

The presence of a secondary vertex provides the most powerful discrimination between b and non-b jets. The kinematic variables of the secondary vertex such as flight distance, direction, track multiplicity, mass or the energy are used in the b-tagging algorithms. The *Simple Secondary Vertex* (SSV) algorithm uses the significance of the flight distance, the ratio of flight distance to its estimated uncertainty, as the discriminating variable. A more complex algorithm, the *Combined Secondary Vertex* (CSV) algorithm, involves the use of secondary vertices together with track based lifetime information to provide the most efficient discrimination between b and non-b jets.

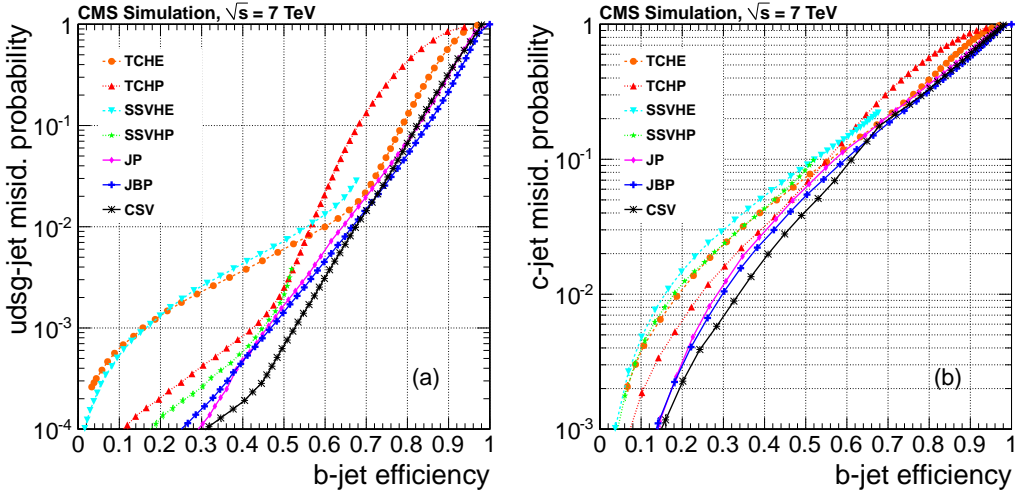


Figure 4: Performance curves obtained from simulation for the algorithms described in the text. (a) light-parton and (b) c-jet misidentification probabilities as a function of the b-jet efficiency

6.2 Performance

The performance of the algorithms discussed above are summarized in Fig. 4 where the misidentification probabilities predicted by simulation are plotted as function of b-jet efficiencies. As seen in Fig. 4, in the region where the misidentification probability is $\sim 10\%$ the JBP algorithm has high b-jet efficiency while in the region where misidentification probability is $< 1\%$ the CSV algorithm is the most efficient. Also the CSV algorithm provides the best c-jet rejection values in the high-purity region.

The efficiency of the b-tagging algorithms are measured from data in order to reduce the dependency on simulation. There are a number of techniques which are applied to CMS data to measure the efficiencies using either dijet events or $t\bar{t}$ events [11]. The dijet events with a jet containing a muon within the jet cone (a “muon jet”) is used to measure the efficiency. A dijet sample with high b-jet purity is obtained by requiring that the “away jet” (other than the muon jet) is b-tagged using a lifetime based b-tagger. Various methods as discussed in [11] are used to measure efficiency using muon-jet events.

The misidentification probability for the light-parton jets is also measured from data relying on the definition of inverted tagging algorithms, selecting non-b jets using the same variables and techniques as the standard versions. The negative tagger is computed from tracks with negative impact parameter or from secondary vertices with negative decay length. The sample of negative tagged jets are enriched with light flavours.

7. Reconstruction and Identification of Electrons and Muons

Electrons are reconstructed by combining tracks in the inner tracker with the energy deposited in the electromagnetic calorimeter. Electron trajectories are reconstructed using a dedicated modeling of the electron energy loss due to bremsstrahlung radiation within the tracker material and are fitted with a Gaussian sum filter [12].

The electrons are identified using track and cluster shape variables such as energy-momentum and the spatial match between the track and the “supercluster” [12], supercluster η width, energy leaked to the hadronic calorimeter. Both cut based and MVA based algorithms are used to combine these variables for electron identification. A series of reference working points are defined depending on the efficiency of electron selection using Monte Carlo samples. The electron isolation variables are computed in three sub-detectors: the tracker, the ECAL, and the HCAL. Transverse momentum/energy sums are evaluated in the region around the electron. To cope with the high event pile-up in 8 TeV data, isolations are computed using particle-flow candidates: charged hadrons, neutral hadrons and photons. Charged hadrons originating from the same primary vertex as the electron are considered for isolation. To account for the neutral energy due to pile-up in the isolation cone, a correction is applied using the pile-up energy density (ρ) estimated on an event by event basis using the jet area method as discussed in Sect.-3.2.

Muons are reconstructed by combining information from muon chambers with that of the inner tracker [13]. Tracks are first reconstructed independently in the inner-tracker (tracker track) and in the muon system (standalone muon track). The standalone muon tracks are matched to the tracker tracks and the hits are combined using a Kalman filter [13] to reconstruct a “global muon”. Tracker only muons are also reconstructed by extrapolating tracks in the inner-tracker to the muon system. If at least one muon segment matches to the extrapolated track, the corresponding tracker track is considered as a “tracker muon”. The muon identification is performed using several categories of muon identification algorithms based on variables such as track quality, compatibility of the calorimeter response with the muon hypothesis, and the presence of matched segments in the muon system. Particle-flow information is also used to improve the purity of the muon identification with substantial low fake rate from charged pions. Several baseline categories of muons are defined based on the analysis requirement. As discussed for electrons, the isolation for muons are also

computed using particle-flow candidates with corrections to account for the neutral energy due to event pile-up.

8. Summary

The CMS experiment has developed excellent techniques for the reconstruction of physics objects by combining information from various components of the CMS detector. The use of the particle-flow technique has greatly improved the reconstruction of hadronic jets, missing transverse energy, and identification of hadronic decay of τ leptons. The particle-flow reconstruction also improved the robustness of the object identification methods against the high event pile-up. The reconstruction and identification of various objects and their performance in data have been briefly presented.

References

- [1] CMS Collaboration, *The CMS experiment at the CERN LHC*, **JINST 3:S08004**.
- [2] CMS Collaboration, *Search for the charged Higgs boson with $H^+ \rightarrow \tau\nu$ decay mode in top quark decays*, **J. High Energy Phys. 07 (2012) 143**; **CMS-HIG-11-019**; **arXiv:1205.5736**.
- [3] CMS Collaboration, *Particle-Flow Event Reconstruction in CMS and Performance for Jets, Taus, and MET*, **CMS-PAS-PFT-09-001**; and references there in.
- [4] CMS Collaboration, *Commissioning of the Particle-Flow reconstruction in Minimum-Bias and Jet Events from pp Collisions at 7 TeV*, **CMS-PAS-PFT-10-002**; and references there in.
- [5] CMS Collaboration, *Jet Performance in pp Collisions at 7 TeV*, **CMS-PAS-JME-10-003**; and references there in.
- [6] M. Cacciari, G. P. Salam, and G. Soyez, "The anti-kt jet clustering algorithm", **JHEP0804:063 (2008)**.
- [7] CMS Collaboration, *The Jet Plus Tracks Algorithm for Calorimeter Jet Energy Corrections in CMS*, **CMS-PAS-JME-09-002**.
- [8] CMS Collaboration, *Determination of Jet Energy Calibration and Transverse Momentum Resolution in CMS*, **J. Instrum. 6 (2011) P11002**; **CMS-JME-10-011**; and references there in.
- [9] CMS Collaboration, *Performance of τ -lepton reconstruction and identification in CMS*, **J. Instrum. 7 (2012) P01001**; **CMS-TAU-11-001**; and references there in.
- [10] CMS Collaboration, *Missing transverse energy performance of the CMS detector*, **J. Instrum. 6 (2011) P09001**; **CMS-JME-10-009**; and references there in.
- [11] CMS Collaboration, *Identification of b-quark jets with the CMS experiment*, **CMS-BTV-12-001**; **arXiv:1211.4462**; and references there in.
- [12] CMS Collaboration, *Electron reconstruction and identification at $\sqrt{s} = 7$ TeV*, **CMS-PAS-EGM-10-001**; and references there in.
- [13] CMS Collaboration, *Performance of CMS muon reconstruction in pp collision events = 7 TeV*, **J. Instrum. 7 (2012) P10002**; **CMS-MUO-10-004**; **arXiv:1206.4071**; and references there in.